

A STUDY ON PREVENTION MEASURES FOR GAUGE CORNER CRACKING

MASAYOSHI OKITA¹, MASAHIRO TSUJIE² & YOSHIAKI TERUMICHI³

¹Graduate School of Sophia University, Japan

²Railway Technical Research Institute, Japan

³Sophia University, Japan

ABSTRACT

There have been many reports of wear and rail damage caused by wheel/rail contact on conventional railway lines in Japan. In particular, rail squats have been commonly reported and gauge corner cracking has been frequently observed on curved high rails with a radius of curvature of approximately 800 m. These forms of damage lead to rail breakage as the cracks develop with the repeated passage of railway vehicles. Predicting crack growth and developing countermeasures is therefore essential for establishing management methods. Furthermore, it is important to reduce the rate of occurrence of these cracks because it is difficult to remove the cracks once they occur. As a countermeasure against rail squats, in addition to the development of a rail grinding method to remove fatigue layers and small cracks on the rail surface, bainitic rails have been developed that promote self-removal of fatigue layers and small cracks by accelerating wear development. However, the advancement of gauge corner cracking is more complicated; for example, gauge corner cracking continuously combines with head checks. At present, countermeasures have not been taken in order to suppress the formation of gauge corner cracking, and there is an urgent need to propose an effective method for doing so. In the present study, countermeasures to reduce gauge corner cracking are proposed by changing the cross-sectional profile of the high rail and reducing the wheel/rail contact pressure and the effectiveness of this method is examined. A mathematical model is constructed from the viewpoint of multi-body dynamics, and the wheel/rail contact pressure at the location at which gauge corner cracking occurs is examined.

Keywords: *contact pressure, creepage, gauge corner cracking, multi-body dynamics, profile prediction, rail damage, wear, wheel/rail contact.*

1 INTRODUCTION

Significant loads and slips by rolling contact with wheels are applied to railway rails. As a result, wear and damage are accumulated on the rail head [1]. Typical examples of rail damage in Japan include rail squats, gauge corner cracking and head checks. In particular, since rail squats and gauge corner cracking can cause rail defects when their growth is significant, rail squats and gauge corner cracking are considered to be a very serious problem for railway safety and stable transportation [2]. In order to suppress the occurrence of rail squats, rail grinding is performed, and bainitic rails, in which the fatigue layer and small cracks are removed by promoting wear, are introduced. In recent years, Thermit head repair welding to remove the damaged portion has also been applied to rail squats. Although gauge corner cracking has been confirmed to occur primarily on high rails with a curvature radius of 800 m, countermeasures for prevention and reduction for wear progress and generation have not yet been proposed. Gauge corner cracks are very difficult to remove completely once they have formed because the cracks are clustered in a continuous manner. Therefore, it is very important to reduce the overall occurrence of gauge corner cracking. In a related study conducted from the viewpoint of material science, a new material for rail construction was tested in order to suppress the gauge corner cracking [3]. The purpose of the present study is to investigate the reduction of the occurrence of gauge corner cracking via the alleviation of the wheel/rail contact pressure.

The authors have constructed a wear progress prediction model using multi-body dynamics in a previous study [4]. In general, it is considered that the shapes of the wheel and rail tend to fit each other as wear develops. Therefore, in the present study, we focused on the state of the wheel/rail contact where the gauge corner cracking occurs by using a wear progress prediction model, and the depression effect on the origin of gauge corner cracking was examined.

2 OCCURRENCE OF GAUGE CORNER CRACKING

In recent years, many occurrences of gauge corner cracking have been confirmed in Japan, mainly in conventional lines with a curvature radius of 800 m. Cracking at the gauge corners of heat-hardened rails on curved high rails continuously occurs combined with head checks (Fig. 1).

Figure 2 shows the rail defects caused by gauge corner cracking. As shown in Fig. 2, rolling contact fatigue cracks occur at the gauge corner on the rail head. Starting from the crack opening on the rail head, the cracks grow as horizontal splits in the longitudinal and horizontal directions of the rail. When the horizontal splits grow greatly, the transverse cracking extends in the vertical direction of the rail branches as well. The branched transverse cracking progresses to the bottom of the rail, leading to rail defects. Thus, the cracks of gauge corner cracking form in a manner similar to rail squats.

Figure 3 shows the fracture surface of the rail defects caused by rail squats. The progress of transverse cracking due to rail squats is approximately line symmetric with respect to the rail central axis. On the other hand, as shown in Fig. 2, the progress area of the transverse cracking due to gauge corner cracking is biased towards the gauge corner. Cracks generated in the rail are detected via ultrasonic using a rail flaw detect car. However, with this

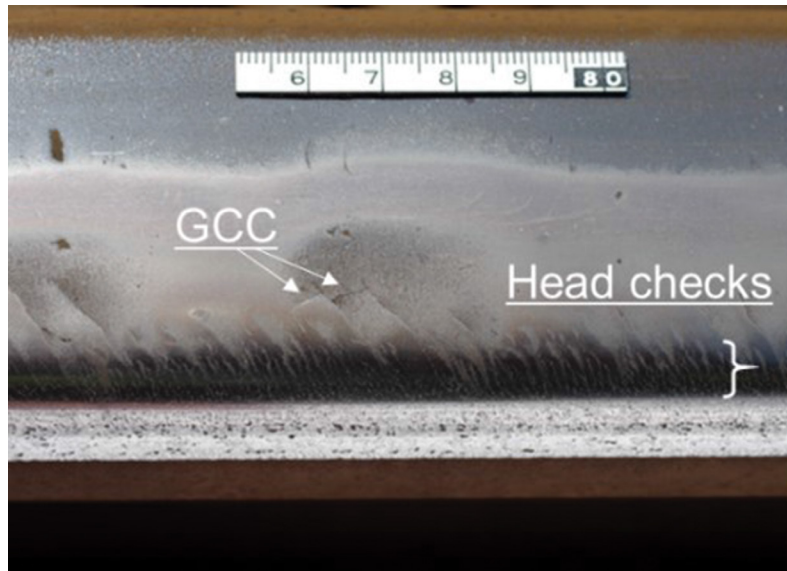


Figure 1: Appearance of gauge corner cracking.

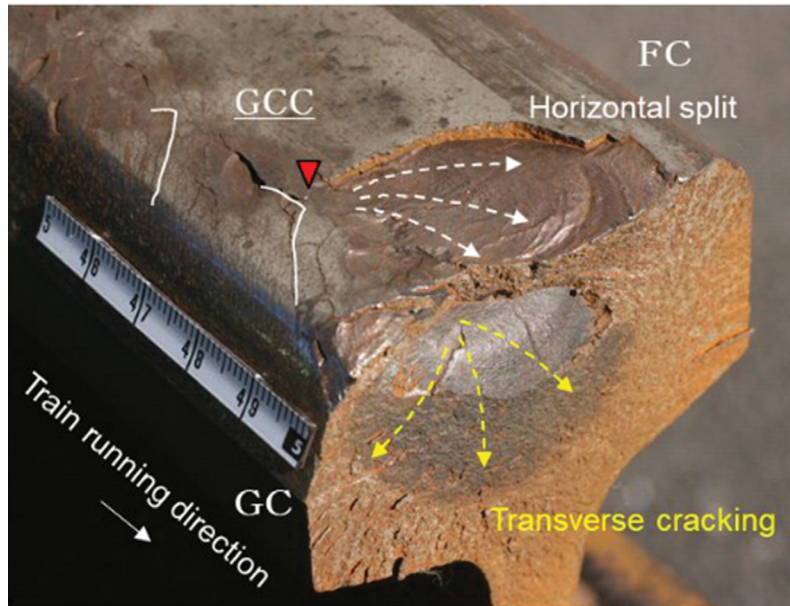


Figure 2: Damage as a result of gauge corner cracking.

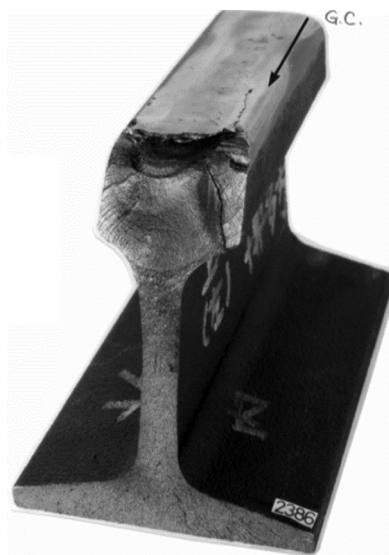


Figure 3: Example of a fracture surface due to rail squats.

method, ultrasonic waves are transmitted only to the centre of the rail in order to transmit the waves all the way through to the bottom of the rail (Fig. 4). Therefore, it is difficult to detect gauge corner cracking in which transverse cracking develops around gauge corners unless the cracks extend to the centre of the rail.

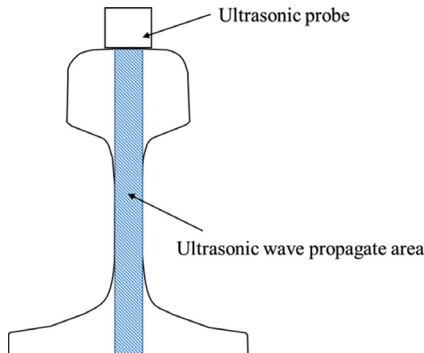


Figure 4: Image of ultrasonic flaw detection.

3 MULTI-BODY DYNAMICS SIMULATION WITH WHEEL/RAIL CONTACT

This section describes the vehicle, wheels and track model simulated using Simpack, which is a multi-body dynamics software. Numerical analysis is performed using the constructed mathematical model in order to describe the wheel/rail contact.

3.1 Analytical model

3.1.1 Vehicle model

A vehicle model which represents a commuter vehicle for business lines in Japan is used for the simulation. As shown in Fig. 5, the model consists of seven bodies: one car body, two bogies and four wheelsets. Each rigid body has six degrees of freedom. However, because the wheelsets are restrained by the contact between the wheel and the rail, they have only four degrees of freedom: longitudinal direction, horizontal direction, pitch angle and yaw angle. Therefore, the proposed vehicle model has 40 degrees of freedom in total. Table 1 also shows the vehicle parameters.

3.1.2 Wheel and rail model

The profiles of the wheels and rail are described by a modified arc and 60-kg rail [5], respectively. The coordinate data that constitutes the cross-sectional shape is composed of 400 monitoring points for wheels and 351 monitoring points for rails with 0.4-mm intervals between each coordinate point. The wheel model does not change its shape in the circumferential direction and one cross-sectional shape is given per wheel model. The rail model was assumed to be rigidly connected to the foundation. The rail model was constructed as shown in Fig. 6, assuming that the rail shape is constant in the longitudinal direction.

3.2 Analysis conditions

The analysis conditions are shown in Table 2, and the track conditions are shown in Table 3. These conditions are based on the running conditions of the curvature radius of 800 m, where gauge corner cracking is most frequently observed. The vehicle passes along the track under the conditions shown in Table 3.

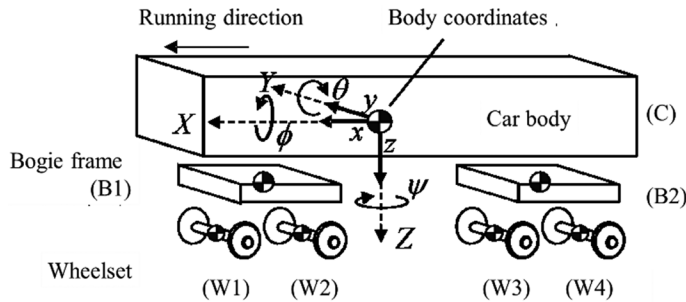


Figure 5: Vehicle model.

Table 1: Vehicle parameters.

Wheelset	[kg]	1,440
Bogies	[kg]	2,095
Car body	[kg]	29,260
Distance between two bogies	[m]	13.8
Wheelbase	[m]	2.1
Distance between two wheel treads	[m]	1.12
Overall length of car body	[m]	20.5
Overall width of car body	[m]	3.1
Overall height of car body	[m]	3.695

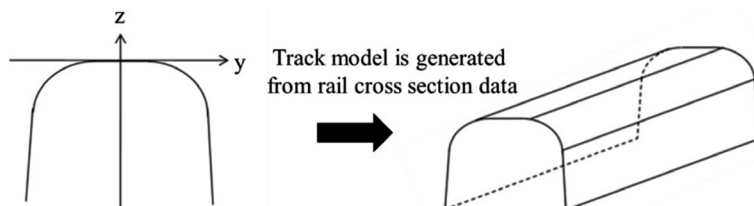


Figure 6: Track model.

Table 2: Analysis conditions.

Velocity	[km/h]	95
Curvature radius	[m]	800
Cant	[mm]	95

Table 3: Track properties.

Straight	[m]	100
Transition curve	[m]	120
Circular curve	[m]	203
Transition curve	[m]	120
Straight	[m]	100

3.3 Numerical simulation of a vehicle travelling on the track

The contact pressure at the curvature radius of 800 m is shown. Since gauge corner cracking is known to occur in the high rail, we focused on the analysis results of the high rail. Figure 7 shows the results for the contact pressure. Wheels 2, 4, 6 and 8 indicate the front and rear wheelsets of the front bogie and the front and rear wheelsets of the rear bogie, respectively. The contact pressure on the front wheelsets of the front and rear bogies each have approximately the same value, and a similar tendency can be seen for the rear wheelsets. In addition, the contact pressure is approximately 700 MPa in the straight part of the rail from 0 to 100 m. In contrast, the contact pressure for the wheels is approximately 1,300 or 1,800 MPa in the curved part of the rail, which is higher than that in the straight part.

4 NUMERICAL SIMULATION OF WEAR PROGRESS

This section outlines the analytical model that integrates the wear prediction model into the numerical analysis model described in Section 3. This model considers only the rail wear without the wheel wear, and we consider the change in wheel contact due to the wear progress.

4.1 Outline of the prediction model for wear progress

4.1.1 Structure

This numerical analysis model by Simpack and the original wear prediction user routine of the model is used. Figure 8 shows the analysis flow of the rail wear shape prediction model.

As shown in Fig. 8, the model of a vehicle and track is simulated using Simpack, and the three-dimensional dynamics analysis and calculations are performed for the contact state, such as the contact force and creepage generated between the wheels and the rails. The numerical results are taken into account in the user routine, and the amount of wear at each monitoring point on the rail is calculated by wheel/rail contact analysis and rail wear calculation. By dividing the amount of wear from the rail cross-sectional shape, the new cross-sectional shape of the rail is formed and reflected in the track model. The dynamics analysis is then performed again using the updated vehicle and track model.

It is possible to calculate the change in the cross-sectional shape of the rail during repeated running by repeating the above series of steps.

4.1.2 Contact pressure

In this section, the contact position and the width of the wheel and rail were calculated by Simpack, and the stress distribution in the contact surface was calculated using the contact radius in the cross-sectional direction based on Hertzian contact theory [6]–[8].

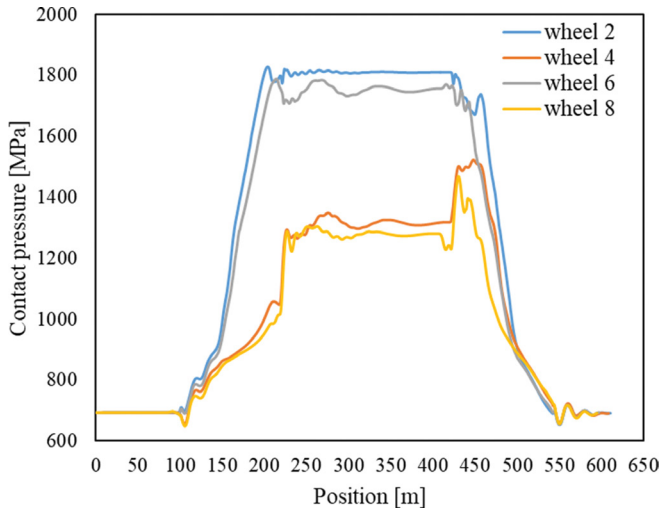


Figure 7: Contact pressure.

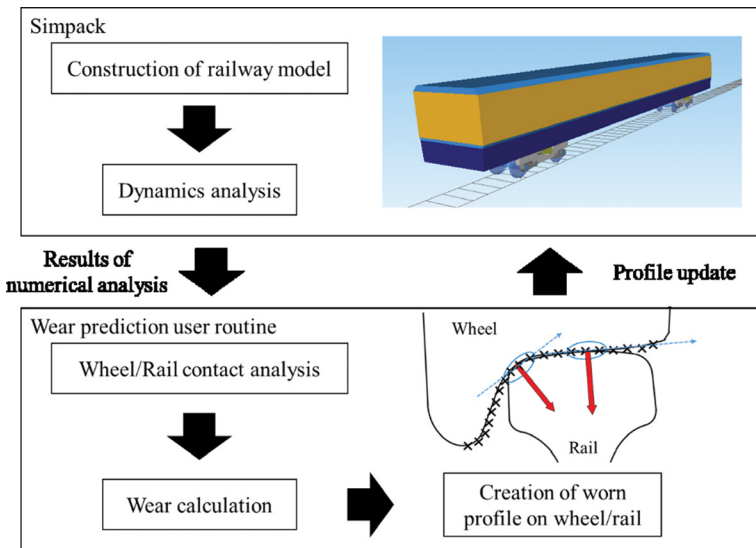


Figure 8: Flowchart of the wear prediction model.

Figure 9 shows a schematic diagram of the contact surface and the contact force between the wheel and the rail. The observation points are set to $i(i=1, 2, 3, \dots)$ in the positive y -axis direction, and the monitoring points on the wheels and rails are set similarly set to $j(j=1, 2, 3, \dots)$. The observation points are on the yz plane of the wheel cross-sectional shape. The axis parallel to the contact surface at each contact point is defined as $\eta(i)$.

Assuming that the number of contact points between the wheels and the rail is Q , the maximum value of the contact pressure $P_{max}(i)[N/m^2]$ is as follows using the contact force $N(i)[N]$ calculated by Simpack:

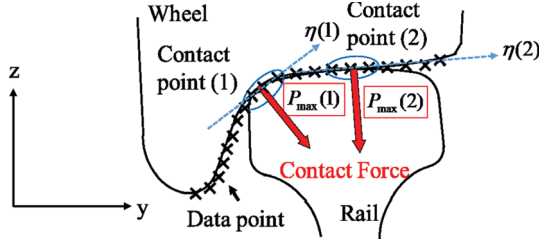


Figure 9: Wheel/rail contact point.

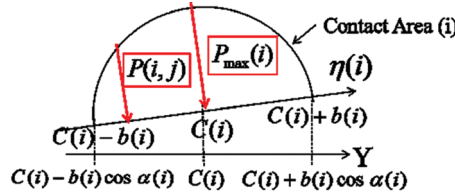


Figure 10: Distribution of contact force.

$$P_{max}(i) = \frac{3N(i)}{2\pi a(i)b(i)} \quad (\text{at } i \le Q) \quad (1)$$

$$P_{max}(i) = 0 \quad (\text{at } i > Q) \quad (2)$$

where $a(i)$ and $b(i)$ [m] are the semi-minor and semi-major axes of the contact ellipse, respectively.

If the angle between the y -axis and the axis η is θ_i , then the contact area on the y -axis is as shown in the following equation and Fig. 10:

$$C(i) - b(i)\cos\theta_i < y(i,j) < C(i) + b(i)\cos\theta_i, \quad (3)$$

where $C(i)$ is the y -coordinate of the centre of the contact point calculated by Simpack, and i is the number of the data points.

As shown in Fig. 10, the contact pressure is expressed as follows:

$$P(i,j) = P_{max}(i) \left[1 - \left(\frac{y(i,j) - C(i)}{b(i)} \right)^2 \right]^{\frac{1}{2}}. \quad (4)$$

4.1.3 Wear model

The wear mode caused by rolling contact between the wheel and the rail is considered to be mainly adhesive wear. Several wear rules for adhesive wear have been proposed [9]–[11]. In the present study, we apply the Archard wear model [12].

$$D = \frac{k \cdot F \cdot s}{H}, \quad (5)$$

where D [m^3] is the wear volume, k [–] is the wear coefficient, F [N] is the contact load, s [m] is the sliding distance and H [N/m^2] is the Vickers hardness.

The wear depth at a certain point is expressed as follows:

$$d(i, j) = \frac{k \cdot P(i, j) \cdot \delta(i)}{H}, \quad (6)$$

where d [m] is the wear depth, P [N/m^2] is the contact pressure and δ [–] is the sliding distance per unit length.

In the present study, the total creepage was calculated using the longitudinal creepage and the lateral creepage obtained by Simpack analysis as follows:

$$\delta(i) = \sqrt{\delta(i)_x^2 + \delta(i)_y^2}. \quad (7)$$

4.1.4 Track model

Since the cross-sectional shapes change over time in the longitudinal direction due to rail wear, we must consider a model that changes shape sequentially. Therefore, we arrange a set point of the cross-section at every meter in the rail longitudinal direction and generate the rail cross-section in the longitudinal direction by performing spline interpolation on the cross-sectional shape of adjacent set points, as shown in Fig. 11.

4.2 Numerical results

The analysis conditions were the same as in Section 3. The amount of wear is calculated based on the contact force and creepage when the vehicle passes over the track once. The amount of wear is then multiplied by 10,000 and is used to generate a new rail profile. The analysis results are the average of 10 continuous rail cross-sections at the centre of the curved section.

Figure 12 shows the rail wear depth at a radius curve of 800 m for 1, 3, 4, 6, 7 and 10 trials. The wear depth was confirmed to not increase at a constant rate with respect to the number of trials, and the increments decreased with the number of trials. It was also confirmed that the wear width became wider as the number of trials increased, indicating that the wear on railway rails is non-linear.

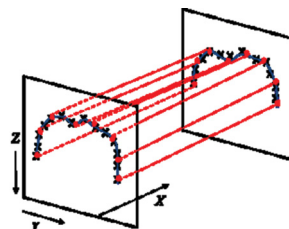


Figure 11: Approximation of rail profile.

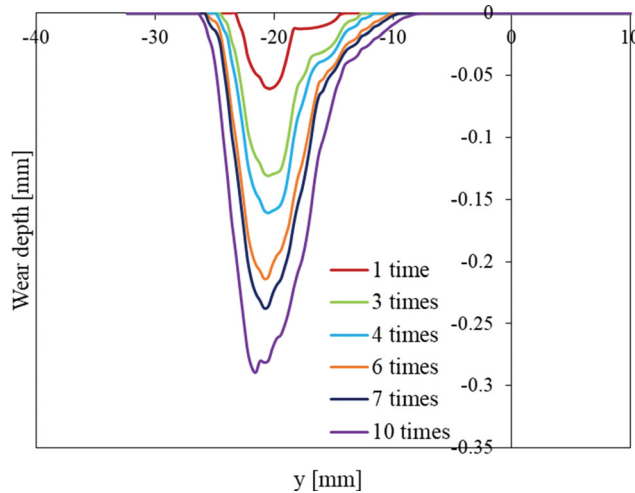


Figure 12: Wear depth.

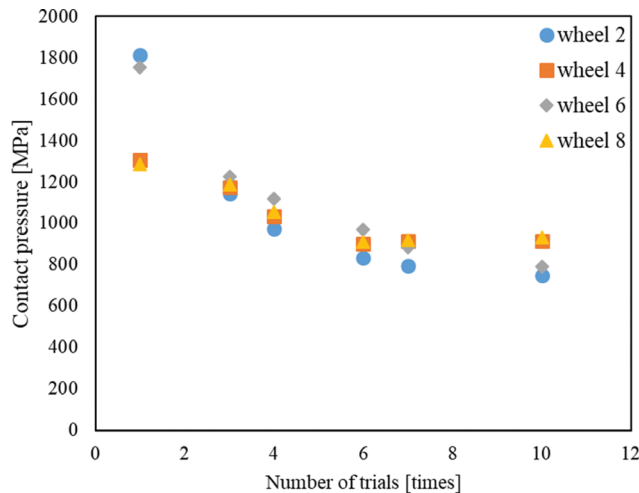


Figure 13: Contact pressure of each wheel.

Next, Fig. 13 shows the contact pressure between each wheel and rail for various numbers of trials. As shown in Fig. 13, the contact pressure for each wheel decreases as the number of trials increases. In addition, the rate of decrease also decreases as the number of trials increases.

Figure 14 shows the creepage between each wheel and rail for various numbers of trials. Here, creepage represents the total creepage calculated using the longitudinal creepage and the lateral creepage occurring on each wheel. As shown in Fig. 14, it can be confirmed that the creepages of wheels 2 and 6 are approximately constant regardless of the number of trials, but the creepages of wheels 4 and 8 decrease as the number of trials increases. The creepages of wheels 4 and 8 in the tenth trial are approximately 60–70% of the initial creepage. In other words, as the rail wear increases, the creepages generated on the rear wheelset of the front and rear bogies decreased by approximately 30–40%, over a duration of up to 10 trials.

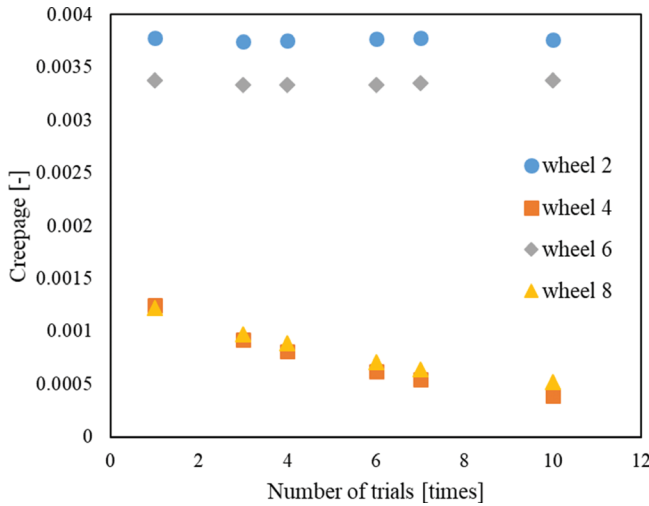


Figure 14: Creepage.

4.3 Discussion

In the present study, we investigated the wheel/rail contact assuming that the wear progresses according to the wear prediction model. As shown in Fig. 13, it can be confirmed that the contact pressure after the sixth trial was approximately constant. This is because the contact area becomes stable as the rail and wheel shapes becomes more closely fitted to each other, and the wear progress rate was found to decrease as the number of trials increased. Moreover, in comparison with the results shown in Figs. 12 and 13, the wear depth was 0.2 mm by the sixth trial, i.e. when the contact pressure reached a steady state. Therefore, the contact pressure can be alleviated by cutting approximately 0.2 mm of depth from the new rail profile, as shown in Fig. 12.

It is necessary to consider the creepage in addition to the contact pressure for the rail damage. The creepage generated at the wheel/rail contact surface on the high rail was examined in order to evaluate the effect on the creepage due to wear progress. It is clear that the creepages of the front wheelset of the front and rear bogies changed only slightly, and that these creepages were not affected by the wear progress (Fig. 14). On the other hand, the creepages of the rear wheelsets decreased approximately 30–40% due to the wear progress. Focusing on the location where the gauge corner cracking occurs on the rail, it was confirmed that the front wheelsets of each bogie runs over that location. Since the creepages of the front wheelset do not change, the creep force acting on the contact position does not change. Therefore, although the creepage does not change, the action of the creep force on the rail damage is considered to be reduced due to the increase in the contact area, so that the shape of worn rail can be expected to have the inhibitory effect on the damage.

In summary, in order to reduce the gauge corner cracking, the effect of the contact pressure of the wheel/rail contact area and the creepage was examined by rail wear progress analysis. It was confirmed that the contact pressure decreased due to the wear progress. Additionally, the creepage did not increase due to the wear progress. Since the shape of

worn rail obtained from the wear progress analysis can alleviate the wheel/rail contact pressure and the creepage, this shape of worn rail can be expected to reduce the occurrence of gauge corner cracking.

5 CONCLUSION

In the present study, we proposed countermeasures by which to reduce gauge corner cracking by changing the cross-sectional profile of the high rail and alleviating the wheel/rail contact pressure. The obtained results are shown below.

- The nonlinearity of wear on railway rails was confirmed. The rate of increase in wear depth and width decreased as the number of trials increased.
- The contact pressure was confirmed to be approximately constant because the wheel and rail shapes were fitted to each other due to the wear progress. As a result, the contact pressure can be reduced by cutting a depth of approximately 0.2 mm from the new rail.
- The gauge corner cracking can be expected to be reduced in the shape of worn rail obtained by the wear progress analysis because the contact pressure between the wheel and the rail and the creepage are alleviated.

REFERENCES

- [1] Magel, E.E., Sawley, K.J., Sroba, P.S. & Kalousek, J., A practical approach to controlling rolling contact fatigue in railways. *8th International Heavy Haul Conference*, pp. 447–455, 2005.
- [2] Grassie, S.L., Rolling contact fatigue on the British railway system: treatment. *WEAR*, 258, pp. 1310–1318, 2005.
- [3] Kanematsu, Y. & Matsui, M., Development and evaluation of the rail steel grade for damage restraint to the high rail in curve sections. *10th International Conference on Contact Mechanics*, 58(1), 2017.
- [4] Yoshioka, A., Terumichi, Y., Tsujie, M. & Matsui, J., Study on modeling and numerical analysis for the prediction of wheel wear development. *Mechanical Engineering Journal*, 4(4), pp. 1–11, 2017.
- [5] Chen, H., Ishida, M., Namura, A., Beak, K.-S., Nakahara, T., Leban, B. & Pau, M., Estimation of wheel/rail adhesion coefficient under wet condition with measured boundary friction coefficient and real contact area. *Wear*, 271, pp. 32–39, 2011.
- [6] Johnson, K.L., *Contact Mechanics*, Cambridge University Press, 1985.
- [7] Kalker, J.J., *Three-Dimensional Elastic Bodies in Rolling Contact*, Kluwer Academic Publishers, 1990.
- [8] Shabana, A.A., Zaazaa, K.E., & Sugiyama, H. *Railroad Vehicle Dynamics: A Computational Approach*, CRC Press, 2008.
- [9] Kalousek, J. & Bethune, A.E., Rail wear under heavy traffic conditions. *ASTM STP644*, pp. 63–79, 1978.
- [10] Ward, A., Lewis, R. & Dwyer-Joyce, R.S., Incorporating a railway wheel wear model into multi-body simulations of wheelset dynamics. *Tribological Research and Design for Engineering Systems*, pp. 367–376, 2003.
- [11] Elkins, J.A. & Eickoff, B.M., Advances in non-linear wheel/rail force prediction methods and their validation. *ASME Winter Annual Meeting*, 1979.
- [12] Archard, J.F., Contact and rubbing of flat surfaces. *Journal of Applied Physics*, 24, pp. 981–988, 1953.